International Journal of Advance Research, IJOAR .org
Volume 1, Issue 6, June 2013, Online: ISSN 2320-9097

CHARGE TRANSPORT IN COLUMBITE PHASE BARIUM NIOBATE

K. N. Singh1, Rajeshwar1 Mishra, P. K. Bajpai2 and A. K. Srivastava1

1Dr. C. V. Raman University, Kota Bilaspur (C.G.) India
2Advance Materials Research Laboratory, Department of Pure and Applied Physics, Guru Ghasidas Vishwavidyalaya, Bilaspur, Chhattisgarh 495009, India
**Author for correspondence: Tel: 91-7752-260249; Mob.: 09685899409 ,*
E-mail: knsingh.ggv@gmail.com

Abstract:

BaNb2O6 (BN) sample was prepared by a high-temperature solid-state reaction route. The material stabilized in orthorhombic with lattice parameters are a=11.9836 A0, b=10.5413 A0, c=7.8822A0. Both ε' and ε" show dispersions at low frequencies and gets almost saturated at higher frequencies. The dispersion in dielectric constant increases with increasing temperature suggests that ac conductivity in BN is due to bulk effect. Single semicircular observed in Nyquist plot of impedance confirms that the polarization completely, from both long-range and localized relaxation which is also confirmed by comparison of M"/M"m and Z"/Z"m analysis. The scaling nature of both Z" and M" implies that the relaxation shows the same mechanism in the entire temperature range. The frequency dependence of conductivity does not follow the simple power law especially at lower frequencies indicating that both translational and relaxational conduction mechanisms are operative. The non-linear fitting of electrical conductivity data using Funke's double power law indicates that reorientation of ions though localized hoping process is dominant conduction mechanism especially at higher temperatures.

Key words*:*

Relaxation, Impedance spectroscopy, Electrical conductivity, Charge transport

1. Introduction:

Alkaline earth and transition metal niobate with general formula MNb_2O_6, where M= Mg, Ca, Sr, Ba, Mn, Fe, Co, Ni, Cu, Zn, Cd, and Pb have been studied [1-7]. Most of MNb_2O_6 compounds can exist as an isomorphs orthorhombic phase with the columbite structure, except for Sr, Ba and Pb analogues which crystallize in a different orthorhombic structure [8, 9]. Microstructure of the alkali-earth metal niobate affects optical properties critically [10]. The microwave dielectric properties of the columbites are to a large extent sensitive to their preparation [11, 12]. Moreover, the synthesis of single phase columbites is often difficult because of the formation of corundum-like crystal phases $A_4Nb_2O_9$ [12]. Barium niobate ($BaNb_2O_6$) is also an important precursor for the preparation of $Sr_xBa_{1-x}Nb_2O_6$ ($0.25 < x < 0.75$) ferroelectric ceramic materials, which have excellent electro-optic, pyroelectric and photorefractive properties [13, 14]. BN is also prepared by urea method [15] particle morphology of calcined powder (600 ^{0}C for 6 h) prepared by this technique was irregular in shape and agglomerated, with an average primary particle size around 85 nm. Most importantly, the techanochemical process can produce powders with nanometer size [16]. High-energy ball milling or mechanochemical processing, which was initially invented for ceramic strengthened alloys [17], has been successfully used to synthesize a wide range of nanosized ceramic powders including $ZnNb_2O_6$ [18], ferroelectrics [19] and $SrAl_2O_4$ [20]. Further, all these reports mainly concerned about the preparation routes and detailed electrical conduction is not studied. For any device application, an understanding of these properties is very much required along with a simple processing route that gives reproducible properties and is low cost with relatively lower temperature processing.

2. Experimental

For preparing $BaNb_2O_6$, Nb_2O_5, $BaCl_2$ and citric acid were used as the starting materials, which were of GR grade (LOBA chem.). A stochiometric amount of $BaCl_2.6H_2O$ was dissolved in distilled water and Nb_2O_5 was dissolved in minimum amount of HF after heating in hot water bath with magnetic stirrer for 14 Hrs. This NbF_5 solution and $BaCl_2 \cdot 2H_2O$ is added and mixed well. A required quantity of HCl was added (drop wise) to dissolve BaF_2 formed by mixing of NbF_5 and $BaCl_2 \cdot 2H_2O$. The above mixture was mixed with required quantity citric acid. pH of solution maintained around 7-7.7. On heating in a water bath at 100^0C a light yellowish gel was formed after evaporation of water. The gel was decomposed at 300^0C. The dried powder was calcined at different temperatures 500 to 800 ^{0}C for 6 h. Fine calcined powders were pressed into disc-shaped pellets at an iso-static pressure of 300 MPa. Polyvinyl alcohol (PVA) was used as a binder. The pellets were sintered at 900 ^{0}C for 4 hours. To determine the dielectric properties, the sintered samples were electroded with air dried silver paste and heated at 300^0C for 2 hour before measurements were performed. The dielectric and impedance spectroscopic data were recorded using HIOKI 3532 LCR Hi TESTER impedance analyzer.

3. Results and Discussions:

Figure 1 shows the XRD pattern of $BaNb_2O_6$ powder after calcination the citrate precursor powder at 800^0C. With the observed interplanar spacing (d_{obs}) of all the peaks of the XRD pattern, unit cell parameters were estimated using a standard computer software POWDMULT. The unit cell with orthorhombic crystal system was selected for which $\Sigma\Delta\delta = (\Sigma\square d_{obs}\text{-}d_{cal})$ is minimum. The crystal structure of $BaNb_2O_6$ was found to be

orthorhombic with lattice parameters are a=11.9836 A^0, b=10.5413 A^0, c=7.8822A^0. All the d-line matches well with reported values (JCPDS: 14-27).

The frequency dependence of real (ε') and imaginary (ε") part of dielectric constant on a log-log plot at different temperatures are shown in Fig.2 The real part of dielectric constant start with higher value than its imaginary part up to 200^0C, and both decreases with increase in frequency; thus plots at (T<200^0C) temperatures are not shown. With further increase in temperature, there is a sudden rise in imaginary part (ε") and it starts with higher value than ε', intersecting at 200Hz at 250^0C. Intersecting frequency shift towards higher frequency as temperature increased (4 kHz at 350^0C). Higher values of both ε' and ε'' as temperature rises, reveal the effect of space charge polarization and or conducting ion motion. The relatively higher values of ε" at low frequency suggest the free charge motion that may be related to ac conductivity relaxation [21], whereas that of ε' may be associated with the accumulation of charges at the interface between the sample and electrode (space charge polarization) [22-23]. Moreover, with increase in frequency, the ε' and ε" terms becomes almost parallel at higher temperatures. This type of behavior is reported in other conducting ion dielectrics and is associated with ion hoping as the dominant mechanism of dielectric relaxation [24]. Thus, the ion hoping mechanism is playing an important role at elevated temperatures.

Variation of real part of impedance Z′ as a function of angular frequency is shown in Fig. 3(a) at various temperatures. The magnitude of Z′ decreases with increase in frequency as well as temperature indicating an increase in ac conductivity with rise in temperature and frequency. The Z′ values at all measured temperatures merge above 40 kHz. This may be due to release of space charge [25, 26]. Fig. 3(b) shows the variation of the imaginary

part of the impedance Z″ with frequency at different temperatures. In Z″ versus log(ω) peak starts appearing with increase in temperature from 100-300^{0}C and shows asymmetric broadening. The peak shifts towards higher frequency with increasing temperature, indicating the spread of relaxation times and the existence of temperature dependent electrical relaxation phenomena. Probably, high temperature triggers grain boundary relaxation process as is also evident from the asymmetric broadening of the peak [27]. The relaxation frequency obeys the Arrhenius relation given by, $\omega_m = \omega_0 exp[-E\tau/K_BT]$, where ω_0 is a pre-exponential factor as shown in the inset of Fig. 3(b). The calculated activation energy for impedance relaxation is 0.15eV.

To analyze, the impedance data are usually modeled by an ideal equivalent electrical circuit comprising of resistance (*R)* and capacitance (*C).* The circuit consists of series combination of grain and grain boundary elements. The grain circuit consists of parallel combination of grain resistance (*Rg)* and grain capacitance (*Cg)*, whereas the grain boundary consists of the parallel combination of grain boundary resistance (*Rgb)* and grain boundary capacitance (*Cgb)* The equivalent electrical equation can be represented by

$$Z^* = Z' - jZ'' = \frac{1}{R_g^{-1} + j\omega C_g} + \frac{1}{R_{gb}^{-1} + j\omega C_{gb}}, \quad (1)$$

$$Z' = \frac{R_g}{1 + (\omega R_g C_g)^2} + \frac{R_{gb}}{1 + \left(\omega R_{gb} C_{gb}\right)^2} \quad (2)$$

$$Z'' = R_g \left[\frac{\omega R_g C_g}{1 + (\omega R_g C_g)^2}\right] + R_{gb} \left[\frac{\omega R_{gb} C_{gb}}{1 + \left(\omega R_{gb} C_{gb}\right)^2}\right], \quad (3)$$

$$Z'' = R_{gb}\left[\frac{\omega R_{gb}C_{gb}}{1+(\omega R_{gb}C_{gb})^2}\right].$$

The semicircle diameter gives the electrical resistivity of the material at the specified temperature, and the maximum value corresponds to the relaxation frequency. Fig.4 shows complex plane impedance plot, (Z* plot), at temperatures 400, 425 and 450^0C. The plots show semicircular arcs that could be fitted with double RC-equivalent circuit, which indicates that the impedance contribution mainly arising from the grains and grain boundaries.

In the modulus formalism an electric modulus M* is defined in terms of the complex dielectric permittivity [28].The frequency dependence of M′(ω) is shown in Fig.5(a). At low frequency, the value of M′ decreases as the temperature increases and finally reaches the origin above 300^0C. Also at a given temperature, M′ increases with increase in frequency and takes almost a constant value at higher frequency. At low frequency and in the high temperature region, M′ approaches zero, confirming an appreciable electrode and/or ionic polarization [29]. Data exhibit a pronounced relaxation peak for M″(ω) (Fig. 5(b)) that moves towards higher frequencies with increase in temperature. It means the relaxation rate for the process increases with increase in temperature. As a convenient measure of the characteristic relaxation time one can choose the inverse of frequency at the maximum peak position, i.e. $\tau_m = \omega_m^{-1}$. The relaxation time satisfies Arrhenius law (plot shown in the inset of Fig. 5(b)). From the numerical fitting, the value of the activation energy comes out to be 0.32 eV. The value is so different to that obtained from impedance relaxation (0.15eV). The Cole–Cole graphs for the electric moduli at 200 to 450^0C are shown in the inset of Fig. 4. The graph resembles a suppressed semicircle

implying a certain deviation from the pure Debye behavior. We have scaled each M″ by M''_m (M''_m is the peak value of the imaginary part of electric modulus) and each frequency ω by ω_m (ω_m corresponds to the frequency of the peak position of M″ in the M″ versus log ω plots) as shown in the inset of Fig. 5(a). Almost perfect overlap of the curves for all temperatures in to a single master curve indicates that the dynamical processes are less temperature independent. Similar scaling for Z″ with Z''_m and each ω with ω_m also reveals the entire curves collapsing into a single master curve as shown in the inset of Fig. 3(a). The scaling behavior of Z″ and M″ implies that the relaxation is governed by the same mechanism in the entire temperature range.

In the description of experimental data, variation of normalized parameters (M''/M''_m) and ($Z''//Z''_m$) as a function of logarithmic frequency at 250^0 C depicted in Fig. 6. Comparison of the impedance and electrical modulus data allow the determination of the bulk response in term of localized, i.e. defect relaxation and/or non-localized conduction, i.e. ionic or electronic conductivity. The magnitude of mismatch between the peaks of both parameters represents a change in the apparent polarization. The overlapping peak positions of M''/M''_m and Z''/Z''_m curves, in general, provide the evidence of delocalized or long-range relaxation [30]. However, in our case, M''/M''_m and Z''/Z''_m peaks (Fig. 6) do not overlap but are very close, suggesting the contributions from both long-range and localized relaxation.

The frequency variation of ac conductivity (σ_{ac}) at different temperatures is shown in figure 7. The behavior of σ_{ac} with frequency at room temperature exhibits both low and high frequency dispersion phenomena. This obeys the Jonscher's power law; $\sigma(\omega) = \sigma_{dc} + A\omega^n$, where n is the temperature dependent frequency exponent ($0 < n < 1$), A is a

thermally activated quantity; hence electrical conduction of the materials is thermally activated process. According to Jonscher [31], the origin of the frequency dependent conductivity lies in the motion of mobile charge carriers. When a mobile charge carrier hops to a new site from its original position, it remains in a state of displacement between two potential energy minima. After a sufficiently long time, the defect could relax until the two minima of lattice potential energy coincide with the lattice site. Also, the conduction behavior of the materials obeys the power law $\sigma(\omega) \alpha \omega^n$ with a slope of σ_{ac} curve governed by n in the low temperature region. According to Funke [32] the value of n has a physical meaning; $n \leq 1$ involved long range hopping motion, whereas for $n > 1$, the motion involves localized hopping without the species leaving the neighborhood. The frequency at which change in slope takes place is known as hopping frequency (ω_p), which is temperature dependent. The slope change occurs at higher frequency with rise in temperature shown in Fig. 7. The plateau region of the conductivity at higher frequency and temperature may be related to the immobility of space charge [33]. This assumption is reasonable since the space charge effect vanishes at higher temperature and frequency. This typical behavior suggests the presence of hopping mechanism being present in the material.

In general, the frequency dependence of conductivity is explained using the power law relation,

$$\sigma(\omega) = \sigma_{dc} + A\omega^n \qquad (4)$$

where σ_{dc} is the frequency independent conductivity and the coefficient A and exponent n are temperature and material dependent. The term $A\omega^n$ contains ac dependence and characterizes all dispersion phenomena. The exponent n show different dependence with

temperature in different systems i.e. remains constant, decreasing with temperature, increasing with temperature but always varies between 0< n <1. The behavior of σ_{ac} with frequency at room temperature exhibits both low and high frequency dispersion phenomena. This obeys the Jonscher's power law at higher frequencies; hence electrical conduction of the materials is thermally activated process at these frequencies. According to Jonscher [31], the origin of the frequency dependent conductivity lies in the motion of mobile charge carriers. When a mobile charge carrier hops to a new site from its original position, it remains in a state of displacement between two potential energy minima. After a sufficiently long time, the defect could relax until the two minima of lattice potential energy coincide with the lattice site. Using Jonscher's universal relation (equation 4) electrical conductivity data are fitted (not shown here), the frequency dependence of conductivity does not follow the simple power law especially at lower frequencies indicating that both translational and relaxational conduction mechanisms are operative. We therefore attempted to fit the frequency dependence of conductivity to double power law as proposed by Funke [32]

$$\sigma(\omega) = \sigma(0) + B_1\omega^{s1} + B_2\omega^{s2} \qquad (5)$$

In this, the exponent, 0< s_1 <1, characterizes the low frequency region corresponding to translational ion hopping. The exponent, 0 <s_2<2 characterizes the high frequency region, indicating the existence of well localized relaxation/ re-orientational process [32], the corresponding activation energy is ascribed to reorientation ion hopping. The non-linear fitting of electrical conductivity data using Funke's double power law (equation 5) in BN is shown in figure 7 and values of pre-exponential factors B_1 , B_2 and exponents s_1, s_2 as obtained from the fitting are given in table 1. The exponent s_1 decreases sharply and s_2

values increases with increase in temperature. This indicates that reorientation of ions though localized hoping process is dominant conduction mechanism especially at higher temperatures.

Conclusions:

$BaNb_2O_6$ stabilized in orthorhombic with lattice parameters are a=11.9836 A^0, b=10.5413 A^0, c=7.8822A^0. Real and imaginary part of dielectric constant show dispersions at low frequencies and gets almost saturated at higher frequencies. The dispersion in dielectric constant increases with increasing temperature suggests that ac conductivity in BN is due to bulk effect. Double semicircular observed in Nyquist plot of impedance confirms that the polarization completely, from both long-range and localized relaxation which is also confirmed by comparison of M''/M''_m and Z''/Z''_m analysis. The scaling nature of both Z" and M" implies that the relaxation shows the same mechanism in the entire temperature range. The frequency dependence of conductivity does not follow the simple power law especially at lower frequencies indicating that both translational and relaxational conduction mechanisms are operative. The non-linear fitting of electrical conductivity data using Funke's double power law indicates that reorientation of ions though localized hoping process is dominant conduction mechanism especially at higher temperatures.

References:

[1] K. Brandt, Arkiv Kemi Mineral. Geol. **17A** (1943) 15.
[2] H.J.Goldschmidt, Metallurgia **62** (1960) 211.
[3] F. Laves, G. Bayer and A. Panagos, Schweiz Mineral Petrogr. Mitt. **43** (1963) 217.
[4] H. Brusset, R. Mahe and U. Aung Kyi, Mater. Res. Bull. **7** (1972) 1061.
[5] I. Yaeger, A.H. Morrish and B.M. Wanklyn, Phys. Rev.B **15** (1977) 1465.
[6] I. Yaeger, I. Maartense and B.M. Wanklyn, Solid State Commun. **21** (1977) 93.
[7] I. Yaeger, A.H. Morrish, B.M. Wanklyn and B.J. Garrard. Phys. Rev. B **16** (1977) 2289.
[8] H. Brusset, M.Gillier-Pandraud and S.D. Voliotis, Mater. Res. Bull. **6** (1971) 5.
[9] R. Roth, Acta Cryst. **10** (1957) 437.
[10] N. Natarajan, Violet Samuel, Renu Pasricha, V.Ravi , Material Science & Engg. B **117** (2005) 169
[11] R. C. Pullar, , J. D. Breeze, and Alford, N. McN., *J. Am. Ceram. Soc.* **88 (**2005) 2466
[12] A. Ananta, R. Brydson, and N. W. Thomas, *J. Eur. Ceram.Soc.*, **19(**1999)355
[13] Y. Xu, Ferroelectric Materials and their Applications, North-Holland, Amsterdam, 1991, p. 254.
[14] Q.W. Huang, P.L. Wang, Y.B. Cheng, D.S. Yan, Mater. Lett. 56 (2002) 915–920.
[15] S.R. Dhagea, Renu Pasrichab, V. Ravi Materials Letters 59 (2005) 1929– 1931
[16] S. Indris, D. Bork, P. Heitjans, J Mater. Synth. Proc. 8 (3/4) (2000) 245–250.
[17] P.S. Gilman, J.S. Benjamin, Annu. Rev. Mater. Sci. 13 (1983) 279–300.
[18] L.B. Kong, J. Ma, H. Huang, R.F. Zhang, T.S. Zhang, J. Alloy Compd. 347 (2002) 308–313.
[19] G. Nicoara, D. Fratiloiu, M. Nogues, J.L. Dormann, F. Vasiliu, Mater. Sci.Forum. 235–238 (1) (1997) 145–150.
[20] G. Chen, D. Niu, X. Liu, J. Alloy Compd. 381 (2005) 280–283.
[21] K.S. Rao, P.M. Krishan, D.M. Prasad and J.H. Lee, Int. J. Mod. Phys. B 21 (2007) 931.
[22] J.S. Kim and T.K. Song, J.Phys.Soc. Jpn.70 (2001) 3419.
[23] S. Saha and T.P. Sinha, J. Appl. Phys, 99 (2006) 014109.
[24] K. Sambhasiva Rao, D.M. Prasad, P. Murali Krishna B.H. Bindu and K. Suneetha, J. Mat.Sc., 42 (2007) 7363
[25] J. Maier, Solid state Ionics, 157 (2003) 327, 154/155 (2002) 291
[26] K. S. Rao, P. M. Krishna, D. M. Prasad, Physics Status Solidi (b) 244 (2007) 2267
[27] J. Mair, J. Eur. Cer.Soc. 24 (2004) 1343.
[28] P.B. Macedo, C.T. Moynihan, R. Bose, Phys. Chem. Glasses **13** (1972) 171.
[29] N. Hirose, A.R. West, j.Ame. Ceram.Soc. 79, (1996)1633
[30] R. Gerhardt, J. Phys. Chem. Solids 55 (1994) 1491.
[31] A.K. Jonscher, Nature **267** (1977) 673.
[32] K. Funke, Prog. Solid State Chem. **22** (1993) 111.
[33] D.P. Almond, G.K. Duncan, A.R. West, Solid State Ionics **8** (1983) 159.

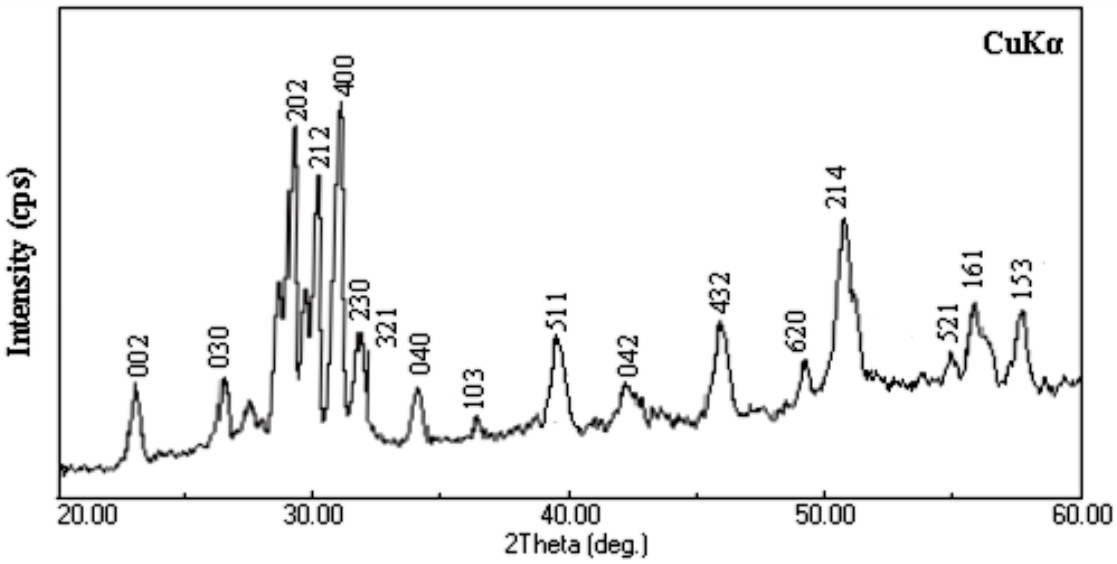

Figure 1 XRD pattern of BaNb2O6 at room temperature.

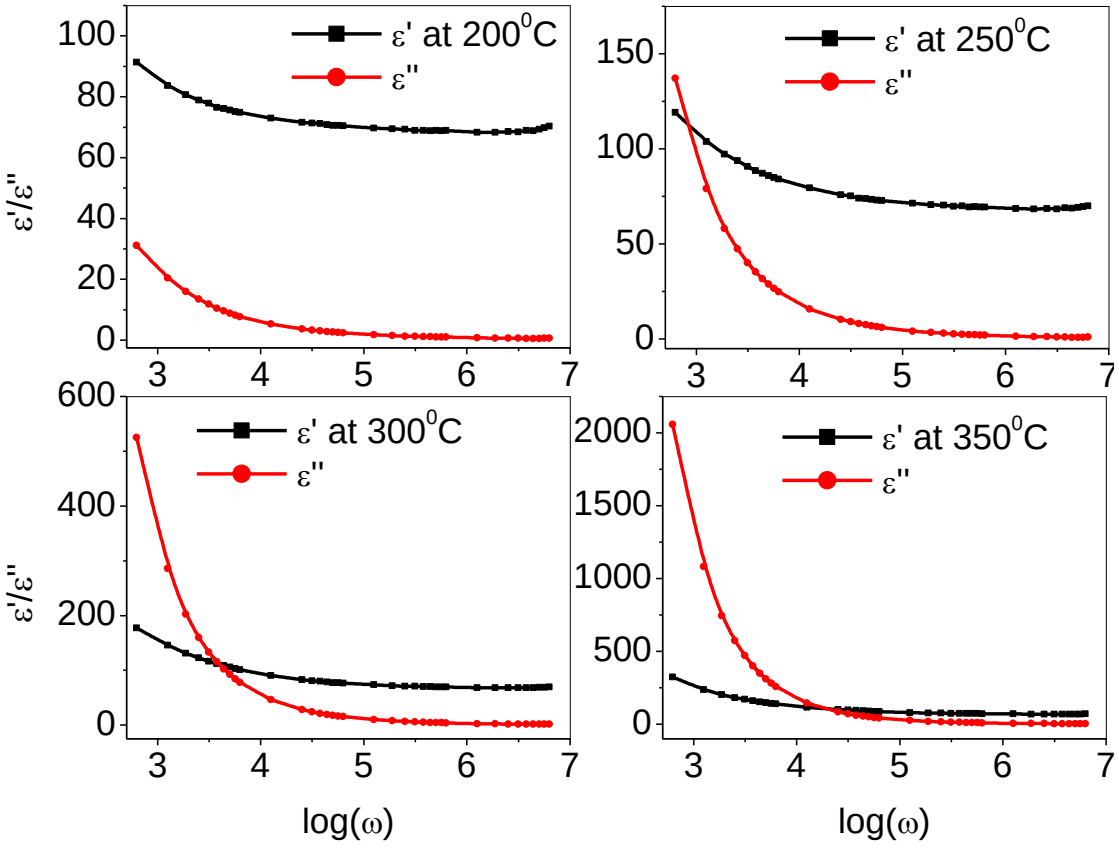

Figure 2. Frequency dependence of real part (ε′) and corresponding imaginary part (ε′′) of dielectric constant at temperature range 200-350^{0}C.

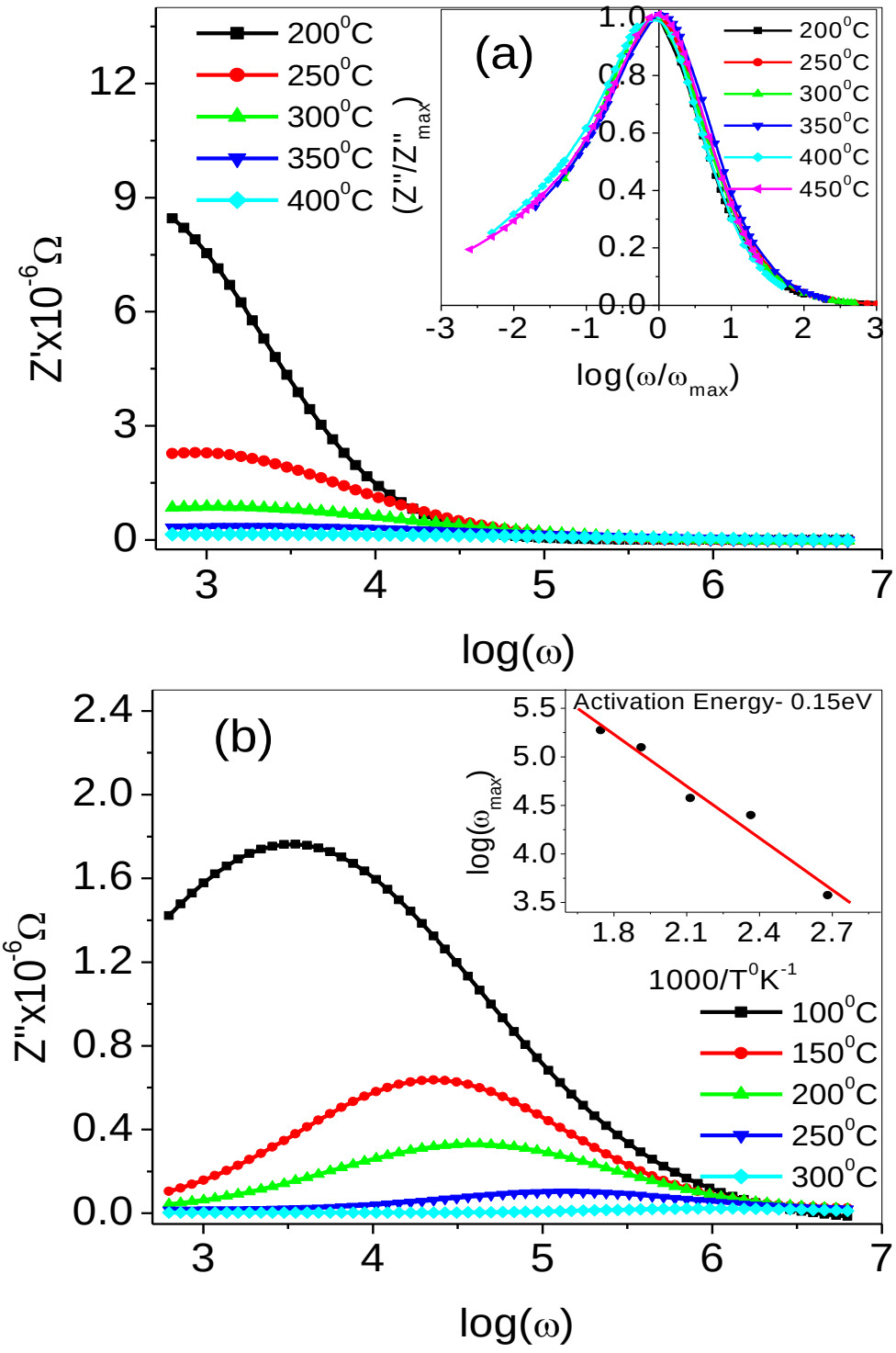

Figure 3. (a) Frequency dependence of real part of impedance (Z′). Inset shows scaling nature of impedance. (b) Frequency dependence of imaginary part of impedance (Z″). Inset shows Arrhenius plots of ω_m corresponding to Z″.

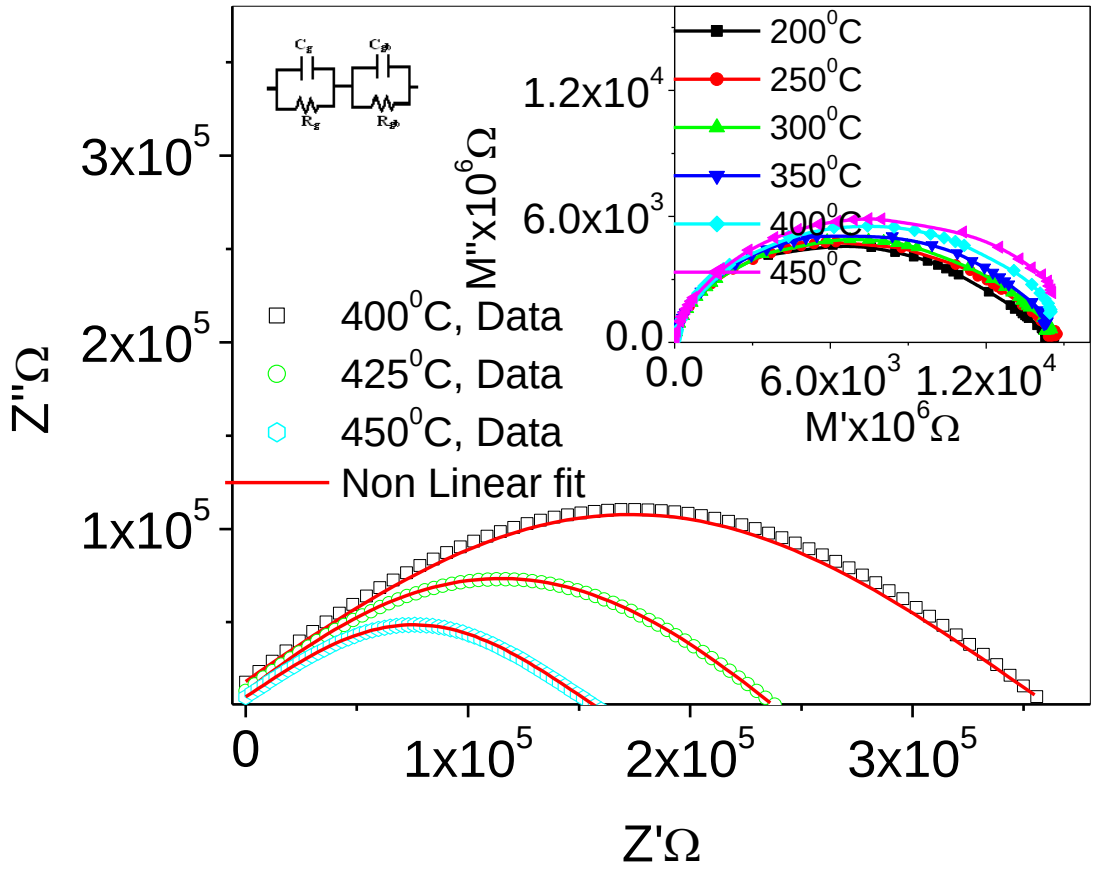

Figure 4. Plots between Z′ and Z″ data along with the NLLS fitting results, using equivalent circuit model proposed for BN. Inset shows complex plane plot of electric modulus.

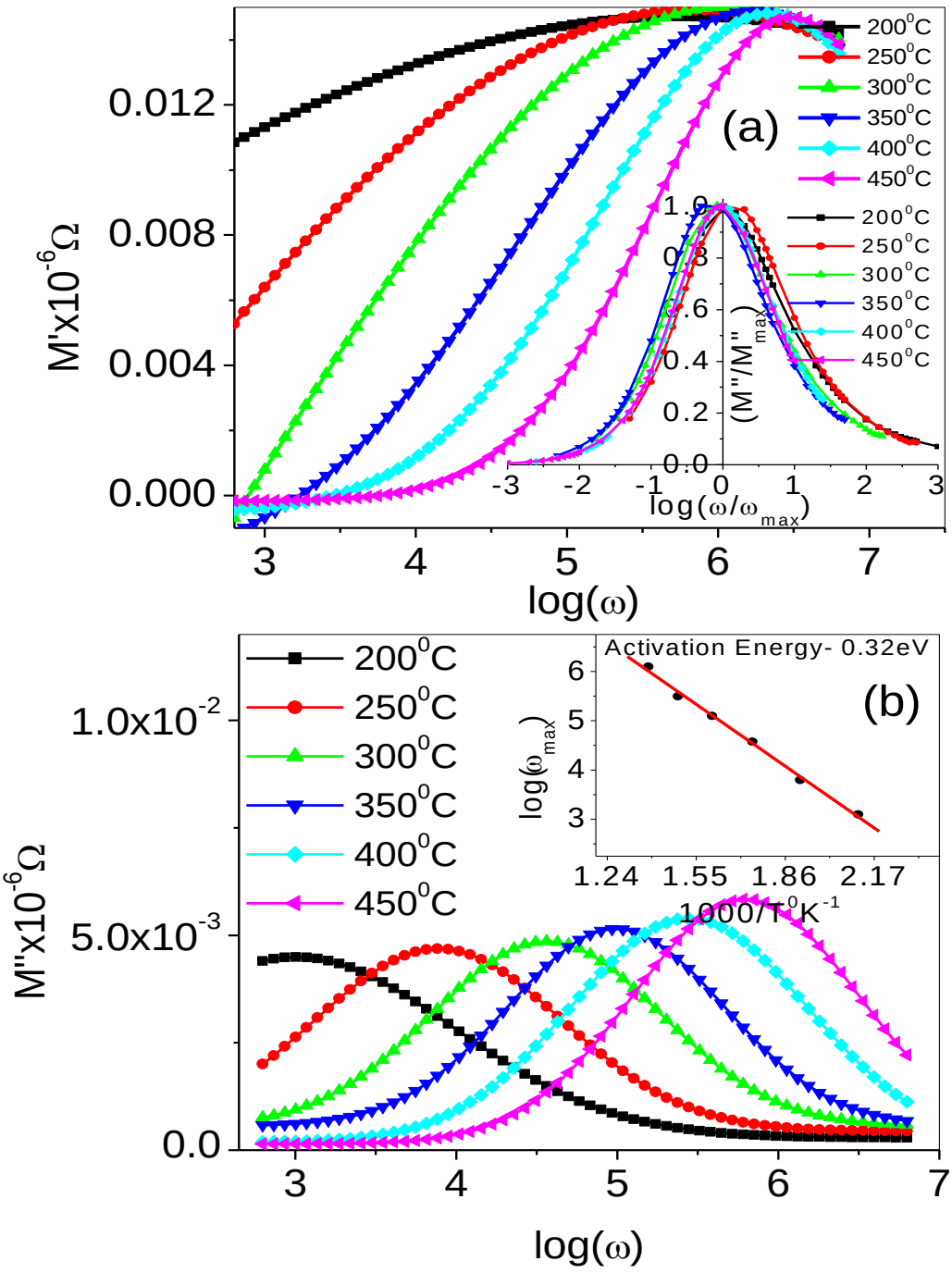

Figure 5. (a) Frequency dependence of M′ at various temperatures for BN. Inset shows scaling nature of electric modulus. (b) Frequency dependence of imaginary part of modulus (M″). Inset shows Arrhenius plots of ω_m corresponding to M″.

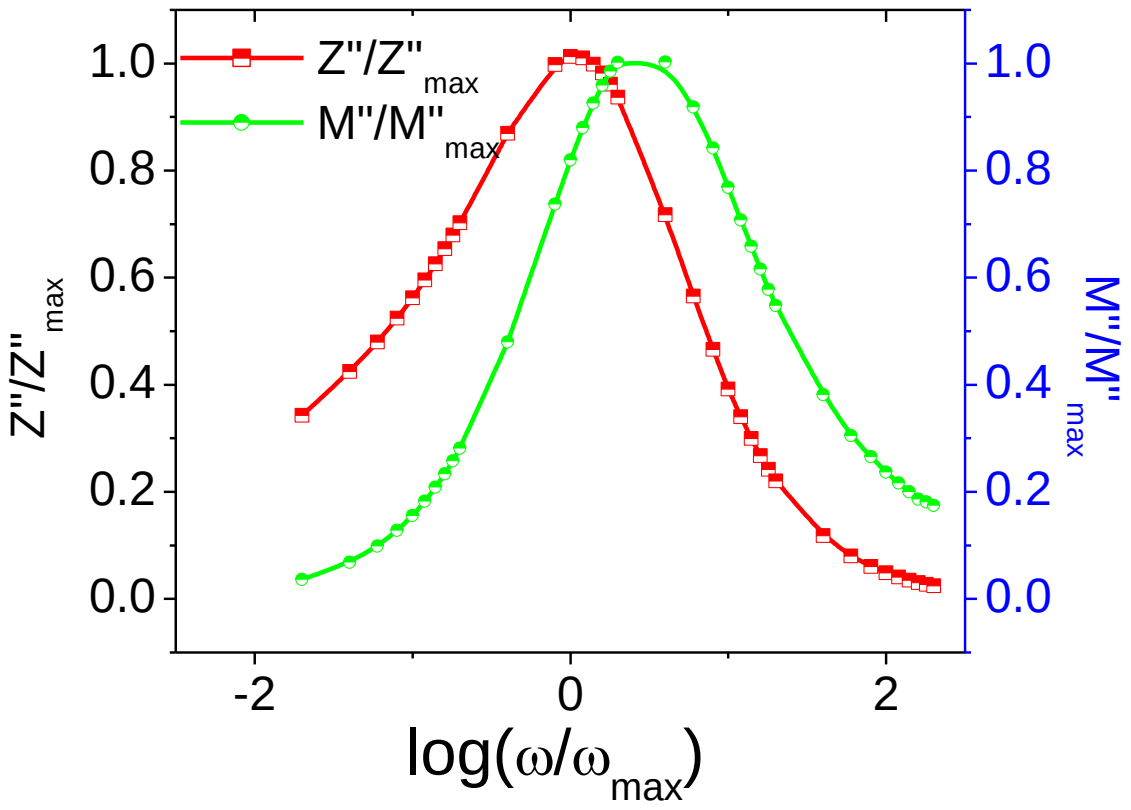

Figure 6. Frequency dependence of normalized imaginary part of electric modulus (M''/M''_m) and impedance (Z''/Z''_m) for BN at 250 ^{0}C.

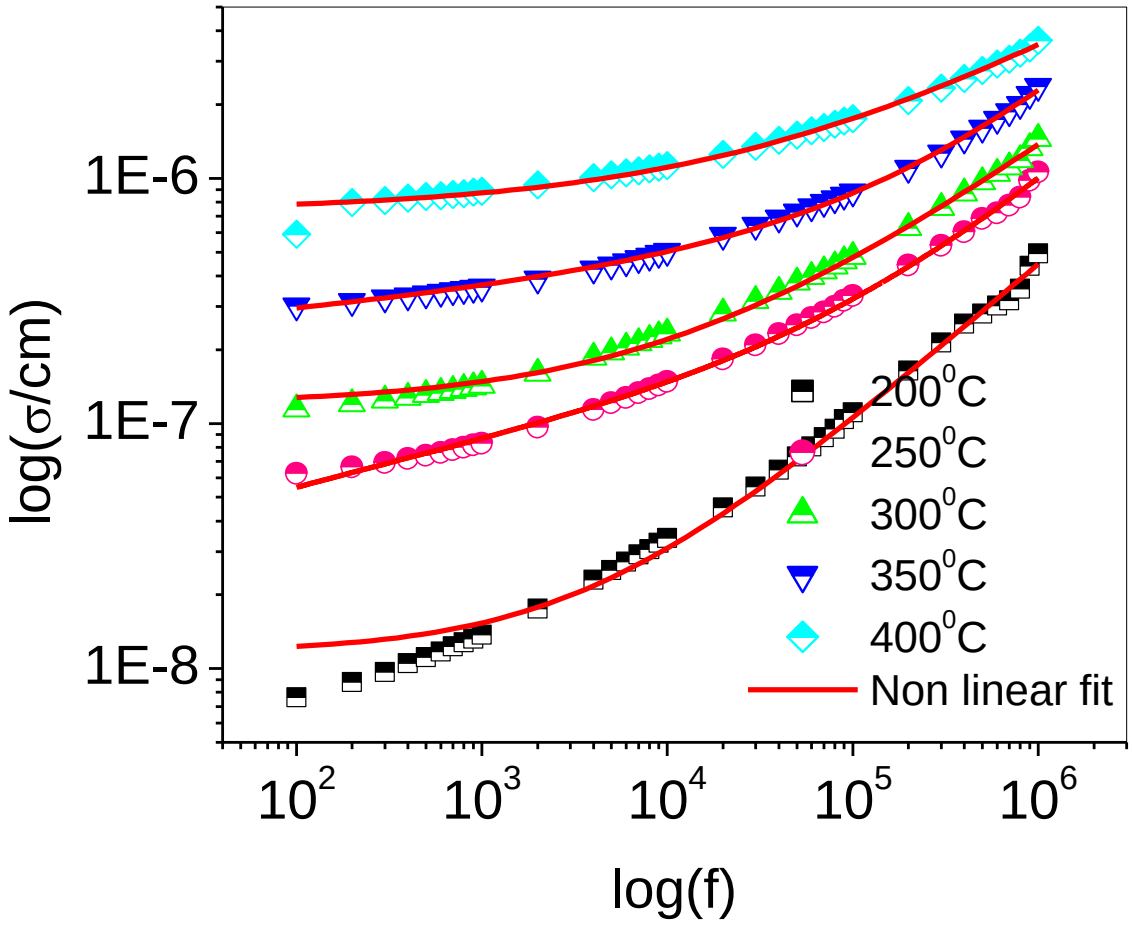

Figure 7. Frequency dependence of the conductivity (σ) for BN at various temperatures where the symbols are the experimental points and the solid lines represent the fitting to the double power law as described in the text.

Table:1 Values of pre-exponential factors B_1 , B_2 and exponents s_1, s_2 as obtained from Nonlinear fitting of electrical conductivity data using Funke's double power law equation $\sigma_{ac} = \sigma_{dc} + B_1\omega^{s1} + B_2\omega^{s2}$ in BN.

Temperature(^{0}C)	**σ_{dc}**	**B_1**	**S_1**	**B_2**	**S_2**
200	1.1767×10^{-8}	2.4265×10^{-10}	0.5489	2.2567×10^{-10}	0.60109
250	4.8065×10^{-8}	7.1133×10^{-10}	0.67478	6.4017×10^{-10}	0.69773
300	1.1934×10^{-7}	3.4951×10^{-10}	0.51707	3.3129×10^{-10}	0.56509
350	1.4085×10^{-7}	7.6965×10^{-8}	0.54871	8.7222×10^{-11}	0.70844
400	7.3438×10^{-7}	3.3997×10^{-9}	0.43495	3.4005×10^{-10}	0.43565